Cellulose

Multi-functional coating of cellulose nanocrystals for flexible packaging applications

--Manuscript Draft--

Manuscript Number:	
Full Title:	Multi-functional coating of cellulose nanocrystals for flexible packaging applications
Article Type:	Original Research
Keywords:	Cellulose nanocrystals (CNs); food packaging; oxygen barrier; anti-fog properties; bio-coating
Corresponding Author:	Fei LI, Ph.D. Università degli Studi di Milano Milan, ITALY
Corresponding Author Secondary Information:	
Corresponding Author's Institution:	Università degli Studi di Milano
Corresponding Author's Secondary Institution:	
First Author:	Fei LI, Ph.D.
First Author Secondary Information:	
Order of Authors:	Fei LI, Ph.D.
	Paolo Biagioni, Ph.D.
	Monica Bollani, Ph.D.
	Andrea Maccagnan
	Luciano Piergiovanni, Professor
Order of Authors Secondary Information:	
Abstract:	In this paper, we systematically address the performance of cellulose nanocrystals (CNs)- coated flexible food packaging films. Firstly, the morphology of CNs from cotton linters and homogeneity of its coating on different substrates were characterized by transmission electronic microscopy and atomic force microscopy. Then, the 1.5 µm thick CNs coating on polyethylene terephthalate (PET), oriented polypropylene (OPP), orientated polyamide (OPA), and cellophane films were characterized for their mechanical, optical, anti-fog, and barrier properties. CNs coating reduces the coefficient of friction while maintaining high transparency (~90%) and low haze (3-4%) values, and shows remarkable oxygen barrier (Oxygen coefficient permeability of CNs coating, KPO2, 0.003 cm3 m-2 24h-1 kPa-1). In addition, the Gelbo flex test combined with PO2 measurements and optical microscopy are firstly reported for evaluating the durability of coatings, revealing that the CNs-coated PET and OPA provide the best performance among the investigated coated films. CNs are therefore considered to be a promising multi-functional coating for flexible food packaging.
Suggested Reviewers:	Tsuguyuki Saito, Ph. D. Assistant Professor, The University of Tokyo asaitot@mail.ecc.u-tokyo.ac.jp He is an expert of TEMPO cellulose nanofibres and has plenty of publications on nano-cellulose applications including coating.
	Nathalie GONTARD, Ph. D. Professor, Université Montpellier II guillard@univ-montp2.fr She is a food packaging expert who is researching on new packaging materials with nanotechnology.
	José M. Kenny, Ph. D. Professor, University of Pergia

	jkenny@unipg.it He leads his group working on bionanocomposites including using the cellulose nanocrystals.
	Markus Linder, Ph. D. Professor , VTT markus.linder@vtt.fi He has been working on nano-cellulose for many years and has plenty of publications on it.

Cover letter

Milan, 21st Mar., 2013

Dear Editor,

I am pleased to enclose here an electronic copy of the original research manuscript entitled "Multi-functional coating of cellulose nanocrystals for flexible packaging applications" for publication on *Cellulose*.

The present manuscript describes the morphology and multiple functions of cellulose nanocrystals (CNs) which is a safe and sustainable nano-material produced from cotton linters by acid-hydrolysis method. Such thin CNs coating significantly improves the mechanical, anti-fog, and barrier properties, while maintaining excellent optical properties.

Firstly, CNs dispersion is coated on four different conventional flexible packaging materials, including polyethylene terephthalate (PET), oriented polypropylene (OPP), oriented polyamide (OPA), and cellophane (CELL). The morphology and homogeneity of CNs coating on different substrates were characterized by atomic force microscopy (AFM). Secondly, the uniform CNs coating (a) reduces the coefficient of friction (COF) resulting in less opportunity of bio-film formation; (b) maintains high transparency and low haze values so that the customers can clearly see the products inside; (c) exhibits excellent anti-fog property determined by calculated surface energy and its components from static and dynamic contact angles values; (d) performs very good oxygen barrier even after Gelbo flex test and improves the water vapour barrier. In addition, we find that the long entangled cellulose fibres are not the only crucial point for obtaining high gas barrier and that different COF and oxygen permeability are attributed to the interaction between CNs and various substrates. We conclude that a multi-functional CNs coating is promising for flexible packaging applications. Therefore, we are expecting that publishing on *Cellulose* might strongly contribute and accelerate technology transfer in this specific field.

The Authors understand the objectives of *Cellulose* and I have formatted the manuscript to fit the style and the needs of the Journal. We also understand the procedure that will be followed in the review process. I declare that the manuscript has been prepared for and sent only to *Cellulose* for publication consideration and it has not been submitted to any other Journal at this time. I attest to the fact that all Authors listed on the title page have directly participated in the planning, execution, and in the discussion of the results of this study. They also have read the manuscript, attested to the validity and legitimacy of the data and their interpretation, and agree to its submission to *Cellulose*. Also, we prefer "Free online colour".

I hope that you consider this manuscript. If there is anything else that you would like to know, please don't hesitate to get in touch with me.

Looking forward to hearing from you soon.

Best regards,

Fei LI
DeFENS, Department of Food, Environmental and Nutritional Sciences – Packaging Division
Università degli Studi di Milano
Via Celoria, 2 20133 MILAN, ITALY
tel. + 39 02 50316654
fax + 39 02 50316672
fei.li@unimi.it
www.defens.unimi.it
http://users.unimi.it/packlab

Multi-functional coating of cellulose nanocrystals for flexible packaging applications

Fei Li, [a*] Paolo Biagioni,[b] Monica Bollani,[c] Andrea.Maccagnan,[d] Luciano Piergiovanni[a]

[a] *DeFENS – Department of Food, Environmental and Nutritional Sciences – Packaging Division, Università degli Studi di Milano, Via Celoria, 2 - 20133 Milano – Italy*

[b] *Dipartimento di Fisica and CNISM, Politecnico di Milano, Piazza L. da Vinci, 32 - 20133 Milano – Italy*

[c] *IFN-CNR, L-NESS, via Anzani 42, 22100 Como – Italy*

[d] *Packaging Division, GOGLIO S.p.A., Via dell'Industria 7 21020 Daverio (VA) – Italy*

* *Corresponding author:*

E-mail: fei.li@unimi.it

Telephone: +39 02.50316654

Fax: +39 02.50316672

Abstract

In this paper, we systematically address the performance of cellulose nanocrystals (CNs)- coated flexible food packaging films. Firstly, the morphology of CNs from cotton linters and homogeneity of its coating on different substrates were characterized by transmission electronic microscopy and atomic force microscopy. Then, the 1.5 µm thick CNs coating on polyethylene terephthalate (PET), oriented polypropylene (OPP), orientated polyamide (OPA), and cellophane films were characterized for their mechanical, optical, anti-fog, and barrier properties. CNs coating reduces the coefficient of friction while maintaining high transparency (~90%) and low haze (3-4%) values, and shows remarkable oxygen barrier (Oxygen coefficient permeability of CNs coating, KPO2, 0.003 cm^3 m^{-2} $24h^{-1}$ kPa^{-1}). In addition, the Gelbo flex test combined with PO2 measurements and optical microscopy are firstly reported for evaluating the durability of coatings, revealing that the CNs-coated PET and OPA provide the best performance among the investigated coated films. CNs are therefore considered to be a promising multi-functional coating for flexible food packaging.

Keywords: Cellulose nanocrystals (CNs); food packaging; oxygen barrier; anti-fog properties; bio-coating

Introduction

Nowadays, the vast majority of food packaging materials is constituted of petrol-based plastics, increasing the dependency of the global economy on fossil resources. Therefore, considering also environmental problems, the interest in bio-based materials, such as poly lactic acid (PLA) (Vert et al., 1995, Drumright et al., 2000, Auras et al., 2004, Lim et al., 2008), starch (Tharanathan, 2003, Avella et al., 2005) or other bio-polymers (Cha and Chinnan, 2004, No et al., 2007, Rhim and Ng, 2007, Hansen and Plackett, 2008, Muzzarelli et al., 2012) has recently been hugely rising. However, such materials are not yet widely applicable because of their inferior properties (Ray et al., 2002, Krikorian and Pochan, 2003, Ray et al., 2003) and high cost, compared with conventional ones, and still many challenges exist before substituting bio-based materials for conventional plastics.

The use of plastic materials for flexible food packaging also poses a challenge in finding appropriate strategies to improve their barrier properties. In current research, inorganic coating, such as aluminum (Chatham, 1996, Lange and Wyser, 2003) and SiO_2 (Erlat et al., 1999, Haas et al., 1999, Creatore et al., 2002) or nano-clays fillers (Sánchez-Valdes et al., 2006, Priolo et al., 2010, Ghasemi et al., 2012, Svagan et al., 2012), are used as oxygen or water vapor barriers with inevitable disadvantages that include a tendency to crack (Priolo et al., 2010) and potential health risks (Lordan et al., 2011). Therefore, a sound strategy consists in partially replacing conventional petrol-based plastics with bio-based materials, for instance, utilizing bio-coatings with the two-fold aim of improving the original plastic properties and reducing the plastic use. Bio-coatings can, therefore, be considered as one of the suitable solutions for food packaging applications.

Nevertheless, the number of directly related bio-coating publications is still limited. Gelatin (Farris et al., 2009) or pullulan (Farris et al., 2012) have been recently reported as oxygen barriers on PET or OPP plastic films. Isogai and his group (Kato et al., 2005) compared the oxygen barrier properties of 12 μm-thick PET films coated by TEMPO-oxidized microcrystalline cellulose, chitosan and starch, whilst TEMPO-oxidized nano-fiber coatings have been demonstrated as an oxygen barrier on PLA and PET film (Fukuzumi et al., 2009, Fujisawa et al., 2011, Rodionova et al., 2012). Besides cast coating, some research groups successfully improved barrier properties of food packaging materials through layer-by-layer (LbL) assembly (Jang et al., 2008, de Mesquita et al., 2010, Priolo et al., 2010, Zhang and Sun, 2010, Yang et al., 2011, Svagan et al., 2012, Li et al., 2013). However, at present TEMPO-oxidized and LbL coating processes are still difficult to apply at the industrial scale due to their cost and process complexity.

In this work, we investigate the physical, mechanical, and optical properties of a bio-coating made of cellulose nanocrystals (CNs), which can be obtained from the most abundant natural polymer on Earth. Besides the promising results that are discussed throughout the paper, such material brings advantages also in terms of low weight, low cost, and biodegradability. Over the last few years, CNs have been extracted from different original sources by chemical, physical, enzymatic processes, or a combination of them (Siró and Plackett, 2010). However, physical and enzymatic processes imply high cost and high energy consumption, respectively, hence we chose a chemical-hydrolysis method for CNs production from cotton linters and we deposited them on different conventional flexible food packaging materials to produce a multi-functional coating. In particular, we used a dispersion of CNs as the coating material deposited on PET, OPP, OPA and cellophane films. The morphology, coefficient of friction, anti-fog, optical, oxygen barrier and water vapor barrier properties of coated films were measured and systematically interpreted.

Materials and methods

Materials.

Cotton linters were provided by S.S.C.C.P. (Milan, Italy) as the raw material to produce CNs.

Four different plastic substrates were coated and used for experiments: (1) poly(ethylene terephthalate) (PET, 12±0.5 μm thickness), (2) oriented polypropylene (OPP, 20±0.5 μm thickness), (3) oriented polyamide (OPA, 12±0.5 μm thickness), and cellophane (CELL,12±0.5 μm thickness). All plastic films have been provided by Radici Film, San Giorgio di Nogaro, Italy.

Methods.

CNs extraction.

1 wt% Cellulose nanocrystals (CNs) dispersion was produced from cotton linter by a procedure described elsewhere (Li et al., 2013). Briefly, milled cotton linters were hydrolyzed by 64 wt% sulfuric acid with vigorous stirring at 45 °C for 45 minutes. The reaction mixture was diluted with deionized water and then rinsed and centrifuged at 5000 rpm repeatedly until the supernatant became turbid. Further purification was then done by dialysis against deionized water (Molecular Weight Cut Off 12 000 and higher). Sequentially, the suspension was sonicated (UP400S 400 W, Hielscher Co., Germany) to create cellulose crystals of colloidal dimensions. Finally, the suspension was filtered under vacuum with Muktell (grade GF/C, 1.2 μm pore diameter) and Whatman glass microfiber filter (grade GF/F, 0.7 μm pore diameter) to remove contamination and big aggregations. The CNs content of the resulting aqueous suspension was determined by drying

several samples (1 ml each) at 105 °C for 15 min intervals (to avoid decomposition or burning) until weight constancy, giving a cellulose concentration of ~1 wt% and a yield of ~50%. To prepare a given concentration of CNs solution, the resulting CNs dispersion was adjusted to pH ~7 by 1M NaOH(aq), freeze-dried and stored in tightly sealed container under dry conditions for later analysis and experiments.

Particle size distribution

1% CNs dispersion was scanned by a laser diffraction particle size analyzer (Mastersizer 2000, Malvern Instruments), combining a blue source with 470 nm wavelength and a red source with 632.8 nm wavelength.

Preparation of Coating Dispersion.

An 8 wt% CNs water dispersion was obtained by dissolving the CNs into distilled water assisted with ultrasonic treatments until the dispersion became visually homogenous. During the process, the sonication should be carried out every ten minute in water bath to avoid overheating. After recovering to room temperature, the CNs dispersion was coated on different plastic films.

Coated Film Preparation.

According to ASTM D823-07, practice C, the corona-treated sides (external sides) of four different rectangular (25×20 cm^2) plastic films were coated by an automatic film applicator (ref 1137, Sheen Instruments, Kingston, U.K.) at a constant speed of 2.5 mm s^{-1}. Water was evaporated using a constant mild air flow

(25±0.3 °C for 5 min) at a perpendicular distance of 40 cm from the automatic applicator. The coated films were stored under controlled conditions (20±2 °C, 45±2.0% RH) for 24 h, and then stored in sealed anhydrous desiccators for 24 h before analysis. All substrates are distinguished by external (Ex) and internal (In) sides. The external side is the pre-treated part, while the internal side is without corona treatments.

Thickness measurements

For the coating thickness measurement, a 10×10 cm^2 sample (plastic substrate with coating) was cut and weighed (m_1, g). The coating was then removed by running hot water (~70 °C) and the resulting bare film was weighed (m_2, g). The coating thickness (l, μm) was obtained according to the following equation:

$$l = \frac{m_1 - m_2}{\rho} \times 100, \tag{1}$$

where ρ ~1.58 g cm^{-3} is the density of CNs (Mazeau and Heux, 2003). Three measurements were performed for each coating type.

Microscopy

Transmission Electron Microscopy (TEM)

Drops of aqueous dispersions of CNs (0.05 wt%) were deposited on carbon-coated electron microscope grids, negatively stained with uranyl acetate and allowed to dry. The samples were analyzed with a Hitachi Jeol-10084 TEM operated at an accelerating voltage of 80 kV.

Atomic force microscopy (AFM)

AFM topography images have been acquired in tapping mode with a Veeco Innova instrument. Super-sharp silicon probes (typical radius of curvature 2 nm) have been used for high-resolution imaging of nanocrystals, while standard silicon probes have been employed for large-area scans in order to evaluate the sample roughness.

The root mean square roughness S is calculated as the standard deviation of the topography

($M \times N$ pixels):

$$S = \sqrt{\frac{1}{MN}\sum_{i=i}^{M}\sum_{j=1}^{N}\left|z(x_i, y_j) - \bar{z}\right|^2}, \qquad (2)$$

where $\bar{z}$ is the mean value of the topography $z(x, y)$.

Optical microscopy

Gelbo Flex treated CNs-coated samples were observed using an optical microscope (Micro Nikon Eclipse ME600 Laboratory Imaging; Nikon Instruments, Sesto Fiorentino, Italy) at 5× and 10× magnification. Pieces of film (30 × 30 mm^2) were mounted on a rectangular glass sample holder and observed without any pretreatment. Images were captured by NIS-Element software (Nikon Instruments, Sesto Fiorentino, Italy).

Coefficient of Friction

The static (μ_S) and dynamic (μ_d) friction coefficients were measured by a dynamometer (model Z005, Zwick Roell, Ulm, Germany), in accordance with the standard method ASTM D 1894-87. The software TestXpert V10.11 (Zwick Roell, Ulm, Germany) Master was used for data analysis.

Optical properties

Transparency measurements

The transmittance of the sample was measured at a wavelength of 550 nm, according to the ASTM D 1746-70, by means of a spectro-photometer (model L650, Perkin-Elmer, Milano, Italy).

Haze

Haze was measured in accordance with ASTM D 1003-61 by means of a spectrophotometer (Perkin Elmer L650). The haze values of uncoated and coated films were obtained as:

$$haze = 100 \times \frac{I_S}{I_T}, \qquad (3)$$

where I_s and I_T are the scattered and total transmitted light, respectively.

Contact angle measurements

Contact angles were measured to estimate the surface energies of the tested substrates by OCA 15 Plus angle goniometer (Data Physics Instruments GmbH, Filderstadt, Germany). The software (SCA20 and SCA21) provided by the instrument manufacturer calculate the surface energy based on contact angles measurements. Measurements of static and advancing contact angle were performed at room temperature with two polar liquids and one apolar liquid:

Milli-Q water, formamide (FOM, ≥99.5%, Carlo Erba, Milano, Italy), and diiodomethane (DIM, 99%, Sigma Aldrich), respectively. Each measurement was repeated on at least five different positions for each sample. The surface energies were calculated from the contact angle data at equilibrium by the Van Oss method (van Oss, 2006), which divides the total surface free energy into two components, the dispersive and the polar components, where the polar interactions originate from the Lewis acid-base interactions:

$$\gamma_i^{total} = \gamma_i^D + \gamma_i^P , \tag{4}$$

where

$$\gamma_i^P = 2\sqrt{\gamma_i^+ \gamma_i^-} , \tag{5}$$

The subscripts i indicate the solid ($i=s$) or liquid ($i=l$) phase, and the superscripts refer to the dispersive (D) and polar (P) components of the total surface energy. γ^+ and γ^- are electron-acceptor and donor parts of the Lewis acid-base interactions.

When combined with Young's equation, the equations developed by Chaudhury, Good, and Van Oss yield the equation (van Oss, 2006)

$$\gamma_l (1 + \cos\theta) = 2(\sqrt{\gamma_l^D \gamma_s^D} + \sqrt{\gamma_s^+ \gamma_l^-} + \sqrt{\gamma_s^- \gamma_l^+} , \tag{6}$$

where θ is the contact angle, γ_l is the liquid surface tension (mJ m^{-2}), and γ_s^+, γ_s^- and γ_l^+, γ_l^- are electron-acceptor and donor contributions to the polar component of the solid and liquid, respectively (mJ m^{-2}). The values of the surface tension and its components for each liquid that were used in calculations were determined by Van Oss (van Oss, 2003). Water, formamide, and diiodomethane, with known γ_l^D, γ_l^+,and γ_l^- values (Table 1) and measured contact angle (θ) were used to determine γ_s^D, γ_s^+, and γ_s^- combined with Equation (6). Finally, γ_s^{total} and γ_s^P were calculated from Equation (4) and (5).

Table 1

Oxygen and water vapor permeability (P_{O2} and P_{H2O}) measurements.

The P_{O2} and P_{H2O} of CNs coated plastic films were measured by permeation instruments (MOCON, OX-TRAN® Model 702 and PERMATRAN-W® Model 700) at 23 °C and 0% relative humidity (RH) and at 38 °C and 100% RH difference, complying with ASTM D-3985, F-1927, F-1307 and ASTM F-1249, respectively.

The P_{O2} of the CNs coating in the coated film [i.e., P_{O2}(*Coating*)] was calculated using the following equation:

$$\frac{1}{P_{O2}(coating)} = \frac{1}{P_{O2}(coated\ \ film)} - \frac{1}{P_{O2}(\,film)}, \qquad (7)$$

where P_{O2}(*coated film*) and P_{O2}(*film*) are the oxygen permeabilities for the coated substrate and the bare substrate, respectively.

Gelbo Flex testing

According to slightly modified ASTM F392, the CNs-coated samples were treated by 20 cycles with Gelbo Flex tester (model S/N 80 03 32, VINATORU ENTERPRISES INC, Graham, USA), shown in Fig. 1. Each cycle includes back and forth steps with 440° on long stroke. After treatments, the samples were observed by optical microscopy and the oxygen permeability was measured according to the method above.

Fig. 1

Results and discussion

Morphology

Fig. 2

Fig. 3

The rod-like CNs produced by sulfuric acid hydrolysis of cotton linters were characterized by TEM as shown in Fig. 2. CNs observations obtained from casted diluted dispersion (approximate 0.05 wt%) show individual nanocrystals and some aggregates. The appearance of aggregated elementary crystallites in TEM images is expected due to the high specific area and strong hydrogen bonds established between the CNs. From several TEM images, the mean values of the length (L) and diameter (d) of the isolated CNs were determined to be 120±30 nm and 6±3 nm, respectively, giving an aspect ratio (L/d) ~20. Similar dimensions have been reported in the literature (Angles and Dufresne, 2000, Elazzouzi-Hafraoui et al., 2007). In order to better understand the CNs size distribution, the probability histogram for the particle size distribution of 1% CNs dispersion is shown in Fig. 3. It indicates that the range of the CNs length is from 90 to 160 nm (mean value ~115 nm), which is highly similar with the results obtained from TEM (Fig. 2) and in other references (Habibi et al., 2010). A certain degree of size distribution is inevitable owing to the acid diffusion-controlled nature of the hydrolysis (de Mesquita et al., 2010). However, the results demonstrate that the acidic hydrolysis process is highly reliable and effective to extract relatively uniform CNs from cotton linters.

Fig. 4

Fig. 4 shows high-resolution AFM images of CNs-coated films. The image shows a dense packing and uniform coverage of nanofibers. We therefore conclude that a new CNs layer was homogeneously established on different conventional packaging materials. Dense packing of CNs has been previously described in other reports (Fujisawa et al., 2011). The continuous layer of overlapping CNs fibers (Siró and Plackett, 2010) points towards possible improvements of the oxygen barrier properties of the different substrates, which we will demonstrate and discuss later on. Moreover, we acquired large-area AFM images, as shown in Fig. 5, where CNs cobble-stone pathway-like aggregations appear due to the strong hydrogen bonds. All images are qualitatively very similar with each other. Root-mean-square roughness values calculated from such AFM investigations all lay in a low-value range (6-13 nm), which is definitely more narrow than the one measured for the external side of bare films (2-21 nm, not shown). A low roughness has been correlated to a less opportunity for bio film formation (Shellenberger and Logan, 2001, Li and Logan, 2004, Ringus and Moraru, 2013), thus bacterial fouling occurrence can be likely reduced by such a coating when applied onto rough substrates.

Fig. 5

Coefficient of friction (COF).

Table 2

The values for the coefficient of friction (COF) of CNs-coated films against films are presented in Table 2. By means of the statistical analysis, we again can conclude that the casting deposition created a completely new CNs-coating layer on different substrates with one exception. In fact, it can be clearly noted that three of the investigated systems (coated-PET, OPA, and CELL) present similar values in dynamic (μ_d) COFs, while only CNs-coated OPP is significantly different from the other coated films and close to the bare one, probably due to weak adhesion between CNs coating and OPP surface which leads to the removal of CNs from substrate during dynamic measurements. The COF results and oxygen permeability discussed later indicate that for thin CNs coating a homogenous independent layer was established by cast coating. It is thus concluded that CNs coating results in an improvement for practical applications, because of the reduction of friction between the films, which might represent a premium feature for high-speed packaging machineries.

Optical properties.

Table 3

As for optical properties, the transparency and haze values of bare films are 87-92% and 2.1-3.0%, respectively, while the ones of coated films are 88-91% and

3.3-4.0%. Detailed results in Table 3 show that the CNs-coated films still maintain high transparency, as requested to ensure easy evaluation of the product quality inside the package. Although their haze values increase, the maximum values (4%) are yet within an acceptable range. Overall, the thin CNs coating (~1.5 µm, as determined by weighting the samples) has no significant influences on the optical properties of coated films.

Anti-fog properties.

Besides the COF improvements and maintaining excellent optical properties, empirical boiling water and breathe (Huff) tests both showed that the CNs-coated films have excellent anti-fog properties, which are presented in Fig. 6. Particularly, we deposited CNs directly on different substrates without any primers or any chemicals to guarantee the safety of food contact. In Fig. 6 we show the results for the coated OPP film since OPP is the most hydrophobic material among the substrates under investigation, but very similar results were obtained for all the substrates. We observed the border [blue dashed line in panels (b) and (c)] between bare and coated films by eye inspection. In order to better observe the anti-fog property, we set a black sponge in the water containers, as shown in Fig. 6(b). As known, fog is formed by small discontinuous water droplets that diffuse the incident light, thereby decrease the transparency and increase the haze (Nuraje et al., 2010, Introzzi et al., 2012). Fig. 6 (c), obtained with optical microscopy, presents two parts, an uncoated one with water droplets, which forms fog, and a coated one with a homogeneous water layer without any droplets, which remained transparent. In the following part, we will further interpret the excellent anti-fog properties of CNs-coated films from the comparison of surface energies obtained from contact angle goniometry.

Fig. 6

Table 4a

Table 4b

From Table 4, we could notice that the CNs-coated films show highly similar static contact angles, which indicates that a completely new CNs layer was established through cast coating process. The static contact angles of CNs coated substrates are much lower than the ones of bare substrates, since cellulose chains contain many hydroxyl (-OH) groups leading to its hydrophilicity. Meanwhile, the dynamic contact angles, which might better reveal the real behavior of hydrophilic surfaces, were also determined. Moreover, it was reported that the differences between the advancing and receding contact angles are usually related with surface's roughness and water absorption often observed on natural fibers (Dankovich and Gray, 2011).

We will use contact angles combined with surface energies of CNs coating to interpret the principles behind the anti-fog performance. The static and dynamic contact angle values (Table 4a and b) are in good agreement with results recently presented on nano-cellulose coated or casted films (Dankovich and Gray, 2011). Regarding the anti-fog properties, it was reported that one possible measure of the level of interaction of water with a material is the advancing contact angle and it has been suggested that hydrophilic surfaces with contact angles lower than 40°

should exhibit anti-fog behavior (Briscoe and Galvin, 1991, Howarter and Youngblood, 2008). Indeed, the measured advancing contact angle values (θ_{Water}) of CNs-coated films are about 26-27°.

Fig. 7

To further interpret the anti-fog behavior, we calculated the surface energies values from contact angles, presented in Fig. 7, through Lifshitz-van der Waals/acid-base theory. In the literature, the surface energy of cellulose determined by contact angle measurements is known to be ~55 mJ m^{-2} (Aulin et al., 2009). Also, a value for the surface energy of CNs films on different substrates was reported as high as 65 mJ m^{-2} with ±15% experimental error (Kontturi et al., 2007). These values are consistent with the values obtained in our results of CNs-coated PET and OPP. Contact angles were measured by using water, FOM, and DIM to provide information regarding the contributions of dispersive (D) and polar (P) components to the total surface energy of the substrates. The calculated values in Fig. 7(a) indicate that the dispersive part of the CNs surface energy is larger than the polar contribution as well as the CNs hydrophilic property, we thus further investigate the electron-acceptor and donor components to the polar part of total surface energy shown in Fig. 7(b). From Fig. 7(b), bare PET and OPP have different asymmetric electron-acceptor and donor patterns due to PET and OPP being relatively hydrophilic and hydrophobic, respectively, while the CN-coated PET and OPP have similar asymmetric patterns which disclose that the thin CNs coating results in an independent and homogeneous layer on PET and OPP substrates. This is a common occurrence since, for a given polar substrate, a strong asymmetry is usually observed between the contribution of electron-acceptor and electron-donor interactions, making one of the two dominant (van Oss, 2006). Furthermore, the electron-donor component (γ_s^-) values of coated PET and OPP shown in Fig. 7(b) are at least 5 and 2000 times the bare ones, which is likely the fundamental factor for different anti-fog performances between bare and coated films. Also, cellulose always presents a polar and hydrophilic surface (Moon et al., 2011) and CNs are grafted with a few sulfate ester groups ($-O-SO_3^-$) due to the sulfuric acid hydrolysis process. These results, therefore, suggest that the anti-fog property induced on the PET and OPP substrates should be attributed to the electron-donor parameter of the polar component. For hydrophilic biopolymers, similar results were also reported (Nuraje et al., 2010, Introzzi et al., 2012).

Barrier properties.

Fig. 8

In addition to excellent performances on COF, optical, and anti-fog properties, the CNs barrier function is evaluated as follows. Fig. 8(a) shows that the oxygen barrier properties of coated films improve significantly thanks to the thin (1.5 µm) CNs coating. The coatings allow for a dramatic reduction (>99%) of oxygen permeability (P_{O2}) of all CNs-coated samples. Oxygen permeability coefficient (KP_{O2}) of CNs coating on OPA is down to 0.003 cm^3 µm m^{-2} $24h^{-1}$ kPa^{-1}, which is much lower than that of commercialized oxygen barrier, ethylene vinyl alcohol (EVOH), under dry condition (Lee et al., 2008). Also, this KP_{O2} value is comparable with the best oxygen barrier from wood TEMPO-oxidized cellulose nanofiber (TOCN-COONa) (Fukuzumi et al., 2011) and this is, according to our best knowledge, the first systematic report on P_{O2} of CNs-coated films. Such excellent oxygen barrier properties achieved on CNs-coated OPA can be tentatively attributed to the strong hydrogen bonds among CNs and between CNs and OPA. We also calculated the KP_{O2} of CNs coatings applied on other substrates, finding always an improved barrier compared to the bare substrate. Therefore, our results indicate that CNs coating provides very good oxygen barrier (especially under dry conditions) but also that the effectiveness of this property is related to the possible interactions between CNs and different plastic films used as coating substrates. One more interesting point is the achievement of high oxygen barrier using short CNs (~120 nm). In other words it seems to be demonstrated that long entangled cellulose fibers (Belbekhouche et al., 2011) are not the only crucial point in achieving certain functionalities.

The P_{O2} of CNs-coated films after Gelbo Flex test is also presented in Fig. 8(a). As known (Habibi et al., 2008, Isogai et al., 2011, Moon et al., 2011), nano-cellulose is stiff and rigid, which should result in fragility of the coating and, thereby, a possible partial loss of the gas barrier properties during usage. Based on the above considerations, we compared the oxygen barrier before and after Gelbo Flex tests. The results indicate that strong distortions led to some destructions of CNs coating and reduce the oxygen barrier properties of all CNs-coated films. Gelbo Flex treated CNs-coated PET and OPA films, however, still maintain a significant low P_{O2}. Compared with others, Gelbo Flex treated coated OPP and cellophane films show relatively higher P_{O2}, probably due to their weak adhesion, which was also observed in dynamic COF tests especially for OPP. In order to confirm this point, we did observations by optical microscopy and the figures are presented in Fig. 9. The morphologies of PET and OPA in Fig. 9 (a), and (c) reveal better adhesions between CNs and PET and OPA, since only a small portion of the CNs film was peeled off from substrates even though there are many chaps (crackles) especially at strongly twisted parts of CNs coatings. However, in case of Gelbo Flex treated CNs-coated OPP, from Fig. 9 (b) we found peeled-off/blister and cracks of CNs coating, which is likely to result in the lower oxygen barrier properties observed. Peeling-off cracks also unexpectedly occurred to cellophane, shown in Fig. 9 (d). This phenomenon might be explained by the presence of resins coated or laminated on the commercialized cellophanes, in this case, low wettable polyester resin. The images from optical microscopy are therefore consistent with the lower oxygen barrier on Gelbo Flex treated coated OPP and cellophane. In this work, the oxygen permeability values were measured only under the dry condition. Since CNs is a hydrophilic biopolymer, the oxygen barrier will be certainly reduced under high RH as other paper reported (Fukuzumi et al., 2012). This limitation is common to the currently used synthetic barrier polymers (polyamide (PA), polyvinyl alcohol (PVOH), ethylene vinyl alcohol (EVOH)) and led to the development of multilayer structures (Li et al., 2013), designed in order to protect moisture sensitive polymers with polyolefin such as low-density polyethylene (LDPE), high-density polyethylene (HDPE), and polypropylene (PP).

The four coated films were also evaluated for their water vapor permeability (P_{H2O}) and Fig. 8(b) reports the results obtained. The P_{H2O} of CNs-coated PET, OPP, OPA and CELL films is reduced by 22, 26, 24 and 6.5% respectively, compared to bare films, while the corresponding thickness increase is 7.5% for OPP and 12.5% for the other three films. Such a limited improvement of the moisture barrier is due to CNs hydrophilicity (Hult et al., 2010, Sanchez-Garcia et al., 2010, Moon et al., 2011) and also to the heavy conditions of the test used (38 °C under a difference of 100% RH). However, the water vapor barrier properties of CNs coating might be satisfactory in real-use conditions which generally involve lower temperature and RH values. Also, high water vapor barrier can already be achieved by conventional and convenient synthetic polymers such as PP and PE.

Fig. 9

Conclusions

To the best of our knowledge, this is the first time that CNs are deposited on different substrates as multi-functional coatings. In the literature, CNs are usually considered as a filler (Noorani et al., 2007, Habibi et al., 2008, Siqueira et al., 2010, Goffin et al., 2011, Dong et al., 2012) or used for small-scale spin or layer-by-layer coating (Kontturi et al., 2007, Cranston and Gray, 2008, Cerclier et al., 2010, Hoeger et al., 2011, Li et al., 2013), and are assumed not to function as a practical coating material (Isogai et al., 2011). In this paper, we systematically investigated the properties of conventional films coated with CNs, demonstrating that CNs coatings mainly lead to a reduction of friction, a premium feature for industrial applications, and that they do not influence significantly the optical properties of coated films. Moreover, CNs coating shows excellent anti-fog property, which is a strongly required performance for flexible food packaging, intended to be used for fresh food. Finally, CNs coatings not only dramatically improve the oxygen barrier properties of conventional flexible food packaging material, but also lead to a certain reduction in the water vapor permeability. While substitution of conventional plastics might still be far ahead because of their low cost, large flexibility and availability, the perspective use of CNs as multi-functional coatings to favor a reduction of the required thickness for plastic films, towards a more environmentally-friendly and sustainable approach to packaging seems promising and feasible. The best substrate to be covered with CNs appeared to be PET and OPA films due to their intrinsic polarity and high surface energies; however, the possible use of activation treatments and other plastic substrates remain to be deeply investigated, as well as the possible measures to reduce the moisture sensitivities and mechanical rigidity of the thin nano-cellulose coatings.

Acknowledgments

We wish to thank Prof. Franco Faoro from Department of Plant Production, Università degli Studi di Milano (Milano, Italy), who carried out TEM observations, Dr. Roberto Galbasini and Dr. Giorgio Bottini, from Goglio S. p. A. (VA, Italy), who helped in oxygen and water vapor barrier measurements, and Dr. Christian Furiosi from SAPICI S. p. A (Milan, Italy), who helped in particle size distribution measurement.

References:

Angles MN and Dufresne A (2000) Plasticized starch/tunicin whiskers nanocomposites. 1. Structural analysis. *Macromolecules* 33, 8344-53.

Aulin C, Ahola S, Josefsson P, Nishino T, Hirose Y, Osterberg M et al. (2009) Nanoscale Cellulose Films with Different Crystallinities and Mesostructures—Their Surface Properties and Interaction with Water. *Langmuir* 25, 7675-85.

Auras R, Harte B, and Selke S (2004) An overview of polylactides as packaging materials. *Macromolecular Bioscience* 4, 835-64.

Avella M, De Vlieger JJ, Errico ME, Fischer S, Vacca P, and Volpe MG (2005) Biodegradable starch/clay nanocomposite films for food packaging applications. *Food Chemistry* 93, 467-74.

Belbekhouche S, Bras J, Siqueira G, Chappey C, Lebrun L, Khelifi B et al. (2011) Water sorption behavior and gas barrier properties of cellulose whiskers and microfibrils films. *Carbohydrate Polymers* 83, 1740-8.

Briscoe BJ and Galvin KP (1991) The effect of surface fog on the transmittance of light. *Solar Energy* 46, 191-7.

Cerclier C, Cousin F, Bizot H, Moreau C, and Cathala B (2010) Elaboration of Spin-Coated Cellulose-Xyloglucan Multilayered Thin Films. *Langmuir* 26, 17248-55.

Cha DS and Chinnan MS (2004) Biopolymer-based antimicrobial packaging: A review. *Critical Reviews in Food Science and Nutrition* 44, 223-37.

Chatham H (1996) Oxygen diffusion barrier properties of transparent oxide coatings on polymeric substrates. *Surface and Coatings Technology* 78, 1-9.

Cranston ED and Gray DG (2008) Birefringence in spin-coated films containing cellulose nanocrystals. *Colloids and Surfaces a-Physicochemical and Engineering Aspects* 325, 44-51.

Creatore M, Palumbo F, and d'Agostino R (2002) Deposition of SiOx films from hexamethyldisiloxane/oxygen radiofrequency glow discharges: Process optimization by plasma diagnostics. *Plasmas and Polymers* 7, 291-310.

Dankovich TA and Gray DG (2011) Contact Angle Measurements on Smooth Nanocrystalline Cellulose (I) Thin Films. *Journal of Adhesion Science and Technology* 25, 699-708.

de Mesquita JP, Donnici CL, and Pereira FV (2010) Biobased Nanocomposites from Layer-by-Layer Assembly of Cellulose Nanowhiskers with Chitosan. *Biomacromolecules* 11, 473-80.

Dong H, Strawhecker KE, Snyder JF, Orlicki JA, Reiner RS, and Rudie AW (2012) Cellulose nanocrystals as a reinforcing material for electrospun poly(methyl methacrylate) fibers: Formation, properties and nanomechanical characterization. *Carbohydrate Polymers* 87, 2488-95.

Drumright RE, Gruber PR, and Henton DE (2000) Polylactic acid technology. *Advanced Materials* 12, 1841-6.

Elazzouzi-Hafraoui S, Nishiyama Y, Putaux J-L, Heux L, Dubreuil F, and Rochas C (2007) The Shape and Size Distribution of Crystalline Nanoparticles Prepared by Acid Hydrolysis of Native Cellulose. *Biomacromolecules* 9, 57-65.

Erlat AG, Spontak RJ, Clarke RP, Robinson TC, Haaland PD, Tropsha Y et al. (1999) SiOx gas barrier coatings on polymer substrates: Morphology and gas transport considerations. *Journal of Physical Chemistry B* 103, 6047-55.

Farris S, Introzzi L, Fuentes-Alventosa JM, Santo N, Rocca R, and Piergiovanni L (2012) Self-Assembled Pullulan-Silica Oxygen Barrier Hybrid Coatings for Food Packaging Applications. *Journal of Agricultural and Food Chemistry* 60, 782-90.

Farris S, Introzzi L, and Piergiovanni L (2009) Evaluation of a bio-coating as a solution to improve barrier, friction and optical properties of plastic films. *Packaging Technology and Science* 22, 69-83.

Fujisawa S, Okita Y, Fukuzumi H, Saito T, and Isogai A (2011) Preparation and characterization of TEMPO-oxidized cellulose nanofibril films with free carboxyl groups. *Carbohydrate Polymers* 84, 579-83.

Fukuzumi H, Saito T, and Isogai A (2012) Influence of TEMPO-oxidized cellulose nanofibril length on film properties. *Carbohydrate Polymers*, http://dx.doi.org/10.1016/j.carbpol.2012.04.069.

Fukuzumi H, Saito T, Iwamoto S, Kumamoto Y, Ohdaira T, Suzuki R et al. (2011) Pore Size Determination of TEMPO-Oxidized Cellulose Nanofibril Films by Positron Annihilation Lifetime Spectroscopy. *Biomacromolecules* 12, 4057-62.

Fukuzumi H, Saito T, Wata T, Kumamoto Y, and Isogai A (2009) Transparent and High Gas Barrier Films of Cellulose Nanofibers Prepared by TEMPO-Mediated Oxidation. *Biomacromolecules* 10, 162-5.

Ghasemi H, Carreau PJ, Kamal MR, and Tabatabaei SH (2012) Properties of PET/clay nanocomposite films. *Polymer Engineering and Science* 52, 420-30.

Goffin AL, Raquez JM, Duquesne E, Siqueira G, Habibi Y, Dufresne A et al. (2011) From Interfacial Ring-Opening Polymerization to Melt Processing of Cellulose Nanowhisker-Filled Polylactide-Based Nanocomposites. *Biomacromolecules* 12, 2456-65.

Haas KH, Amberg-Schwab S, Rose K, and Schottner G (1999) Functionalized coatings based on inorganic-organic polymers (ORMOCER (R) s) and their combination with vapor deposited inorganic thin films. *Surface & Coatings Technology* 111, 72-9.

Habibi Y, Goffin AL, Schiltz N, Duquesne E, Dubois P, and Dufresne A (2008) Bionanocomposites based on poly(epsilon-caprolactone)-grafted cellulose nanocrystals by ring-opening polymerization. *Journal of Materials Chemistry* 18, 5002-10.

Habibi Y, Lucia LA, and Rojas OJ (2010) Cellulose Nanocrystals: Chemistry, Self-Assembly, and Applications. *Chemical Reviews* 110, 3479-500.

Hansen NML and Plackett D (2008) Sustainable films and coatings from hemicelluloses: A review. *Biomacromolecules* 9, 1493-505.

Hoeger I, Rojas OJ, Efimenko K, Velev OD, and Kelley SS (2011) Ultrathin film coatings of aligned cellulose nanocrystals from a convective-shear assembly system and their surface mechanical properties. *Soft Matter* 7, 1957-67.

Howarter JA and Youngblood JP (2008) Self-Cleaning and Next Generation Anti-Fog Surfaces and Coatings. *Macromolecular Rapid Communications* 29, 455-66.

Hult EL, Iotti M, and Lenes M (2010) Efficient approach to high barrier packaging using microfibrillar cellulose and shellac. *Cellulose* 17, 575-86.

Introzzi L, Fuentes-Alventosa JM, Cozzolino CA, Trabattoni S, Tavazzi S, Bianchi CL et al. (2012) "Wetting Enhancer" Pullulan Coating for Antifog Packaging Applications. *ACS Applied Materials & Interfaces* 4, 3692-700.

Isogai A, Saito T, and Fukuzumi H (2011) TEMPO-oxidized cellulose nanofibers. *Nanoscale* 3, 71-85.

Jang W-S, Rawson I, and Grunlan JC (2008) Layer-by-layer assembly of thin film oxygen barrier. *Thin Solid Films* 516, 4819-25.

Kato Y, Kaminaga J-i, Matsuo R, and Isogai A (2005) Oxygen Permeability and Biodegradability of Polyuronic Acids Prepared from Polysaccharides by TEMPO-Mediated Oxidation. *Journal of Polymers and the Environment* 13, 261-6.

Kontturi E, Johansson LS, Kontturi KS, Ahonen P, Thune PC, and Laine J (2007) Cellulose nanocrystal submonolayers by spin coating. *Langmuir* 23, 9674-80.

Krikorian V and Pochan DJ (2003) Poly (L-lactic acid)/layered silicate nanocomposite: Fabrication, characterization, and properties. *Chemistry of Materials* 15, 4317-24.

Lange J and Wyser Y (2003) Recent innovations in barrier technologies for plastic packaging—a review. *Packaging Technology and Science* 16, 149-58.

Lee DS, Yam KL, and Piergiovanni L (2008) In *Food Packaging Science and Technology*. Vol. pp. 58-59, 86-93, CRC Press,

Li B and Logan BE (2004) Bacterial adhesion to glass and metal-oxide surfaces. *Colloids and Surfaces B: Biointerfaces* 36, 81-90.

Li F, Biagioni P, Finazzi M, Tavazzi S, and Piergiovanni L (2013) Tunable green oxygen barrier through layer-by-layer self-assembly of chitosan and cellulose nanocrystals. *Carbohydrate Polymers* 92, 2128-34.

Lim LT, Auras R, and Rubino M (2008) Processing technologies for poly(lactic acid). *Progress in Polymer Science* 33, 820-52.

Lordan S, Kennedy JE, and Higginbotham CL (2011) Cytotoxic effects induced by unmodified and organically modified nanoclays in the human hepatic HepG2 cell line. *Journal of Applied Toxicology* 31, 27-35.

Mazeau K and Heux L (2003) Molecular Dynamics Simulations of Bulk Native Crystalline and Amorphous Structures of Cellulose. *The Journal of Physical Chemistry B* 107, 2394-403.

Moon RJ, Martini A, Nairn J, Simonsen J, and Youngblood J (2011) Cellulose nanomaterials review: structure, properties and nanocomposites. *Chemical Society Reviews* 40, 3941-94.

Muzzarelli RAA, Boudrant J, Meyer D, Manno N, DeMarchis M, and Paoletti MG (2012) Current views on fungal chitin/chitosan, human chitinases, food preservation, glucans, pectins and inulin: A tribute to Henri Braconnot, precursor of the carbohydrate polymers science, on the chitin bicentennial. *Carbohydrate Polymers* 87, 995-1012.

No HK, Meyers SP, Prinyawiwatkul W, and Xu Z (2007) Applications of chitosan for improvement of quality and shelf life of foods: A review. *Journal of Food Science* 72, R87-R100.

Noorani S, Simonsen J, and Atre S (2007) Nano-enabled microtechnology: polysulfone nanocomposites incorporating cellulose nanocrystals. *Cellulose* 14, 577-84.

Nuraje N, Asmatulu R, Cohen RE, and Rubner MF (2010) Durable Antifog Films from Layer-by-Layer Molecularly Blended Hydrophilic Polysaccharides. *Langmuir* 27, 782-91.

Priolo MA, Gamboa D, Holder KM, and Grunlan JC (2010) Super Gas Barrier of Transparent Polymer−Clay Multilayer Ultrathin Films. *Nano Letters* 10, 4970-4.

Ray SS, Yamada K, Okamoto M, and Ueda K (2003) New polylactide-layered silicate nanocomposites. 2. Concurrent improvements of material properties, biodegradability and melt rheology. *Polymer* 44, 857-66.

Ray SS, Yamada K, Okamoto M, and Ueda K (2002) Polylactide-layered silicate nanocomposite: A novel biodegradable material. *Nano Letters* 2, 1093-6.

Rhim J-W and Ng PKW (2007) Natural biopolymer-based nanocomposite films for packaging applications. *Critical Reviews in Food Science and Nutrition* 47, 411-33.

Ringus DL and Moraru CI (2013) Pulsed Ligh inactivation of Listeria innocua on food packaging materials of different surface roughness and reflectivity. *Journal of Food Engineering* 114, 331-7.

Rodionova G, Saito T, Lenes M, Eriksen O, Gregersen O, Fukuzumi H et al. (2012) Mechanical and oxygen barrier properties of films prepared from fibrillated dispersions of TEMPO-oxidized Norway spruce and Eucalyptus pulps. *Cellulose* 19, 705-11.

Sánchez-Valdes S, López-Quintanilla ML, Ramírez-Vargas E, Medellín-Rodríguez FJ, and Gutierrez-Rodriguez JM (2006) Effect of Ionomeric Compatibilizer on Clay Dispersion in Polyethylene/Clay Nanocomposites. *Macromolecular Materials and Engineering* 291, 128-36.

Sanchez-Garcia MD, Hilliou L, and Lagaron JM (2010) Morphology and Water Barrier Properties of Nanobiocomposites of k/i-Hybrid Carrageenan and Cellulose Nanowhiskers. *Journal of Agricultural and Food Chemistry* 58, 12847-57.

Shellenberger K and Logan BE (2001) Effect of Molecular Scale Roughness of Glass Beads on Colloidal and Bacterial Deposition. *Environmental Science & Technology* 36, 184-9.

Siqueira G, Abdillahi H, Bras J, and Dufresne A (2010) High reinforcing capability cellulose nanocrystals extracted from Syngonanthus nitens (Capim Dourado). *Cellulose* 17, 289-98.

Siró I and Plackett D (2010) Microfibrillated cellulose and new nanocomposite materials: a review. *Cellulose* 17, 459-94.

Svagan AJ, Åkesson A, Cárdenas M, Bulut S, Knudsen JC, Risbo J et al. (2012) Transparent Films Based on PLA and Montmorillonite with Tunable Oxygen Barrier Properties. *Biomacromolecules* 13, 397-405.

Tharanathan RN (2003) Biodegradable films and composite coatings: past, present and future. *Trends in Food Science & Technology* 14, 71-8.

van Oss CJ (2006) Interfacial Forces in Aqueous Media. In Dekker M (ed.), pp. 18-28 and 93-107. CRC Press, New York.

van Oss CJ (2003) Long-range and short-range mechanisms of hydrophobic attraction and hydrophilic repulsion in specific and aspecific interactions. *Journal of Molecular Recognition* 16, 177-90.

van Oss CJ, Wu W, Docoslis A, and Giese RF (2001) The interfacial tensions with water and the Lewis acid–base surface tension parameters of polar organic liquids derived from their aqueous solubilities. *Colloids and Surfaces B: Biointerfaces* 20, 87-91.

Vert M, Schwarch G, and Coudane J (1995) Present and Future of PLA Polymers. *Journal of Macromolecular Science-Pure and Applied Chemistry* A32, 787-96.

Yang Y-H, Haile M, Park YT, Malek FA, and Grunlan JC (2011) Super Gas Barrier of All-Polymer Multilayer Thin Films. *Macromolecules* 44, 1450-9.

Zhang L and Sun J (2010) Layer-by-Layer Codeposition of Polyelectrolyte Complexes and Free Polyelectrolytes for the Fabrication of Polymeric Coatings. *Macromolecules* 43, 2413-20.

Figure Caption

Fig. 1 Gelbo Flex tester, a, b, and c indicate different phases of a back and forth cycle.

Fig. 2 TEM image of individual CNs

Fig. 3 Probability histogram for the particle size distribution measured from 1% CNs dispersion

Fig. 4 High-resolution AFM images of CNs-coated PET (a), OPP (b), OPA (c), and CELL (d).

Fig. 5 AFM for roughness of coated substrates, coated PET (a), OPP (b), OPA (c), and cellophane (d).

Fig. 6 Boiling water test; panel (a) the foggy bare OPP observed with an optical microscope; panel (b) comparison between bare and CNs-coated OPP during the test; panel (c) the border between CNs-coated and bare parts observed with an optical microscope.

Fig. 7 Surface energies and their respective polar and dispersive components of bare and CNs-coated PET and OPP, (a); the electron-acceptor and donor of polar component, (b)

Fig. 8 The oxygen permeability (P_{O2}) of bare, CNs-coated, and CNs-coated after Gelbo Flex tests PET, OPP, OPA, and CELL films at 23 °C under dry condition (a); the water vapor permeability of bare and CNs-coated PET, OPP, OPA, and CELL films at 38 °C under 100% RH difference (b).

Fig. 9 The morphology of Gelbo Flex treated CNs-coated PET (a), OPP (b), OPA (c), and CELL (d) films by optical microscopy.

Tables

Table 1 Surface tension components and parameters of the liquids used in direct contact angle determination in mJ m^{-2}, at 20 °C (van Oss et al., 2001, vanOss, 2003)

Table 2 The coefficient of friction (COF) of Plastic films (Ex) against plastic film (In)

Table 3 Transparency at 550 nm and haze of bare and CNs-coated films

Table 4a Static contact angles of bare and CNs-coated films

Table 4b Advancing and receding contact angles of bare and CNs-coated films

Figure1

Click here to download high resolution image

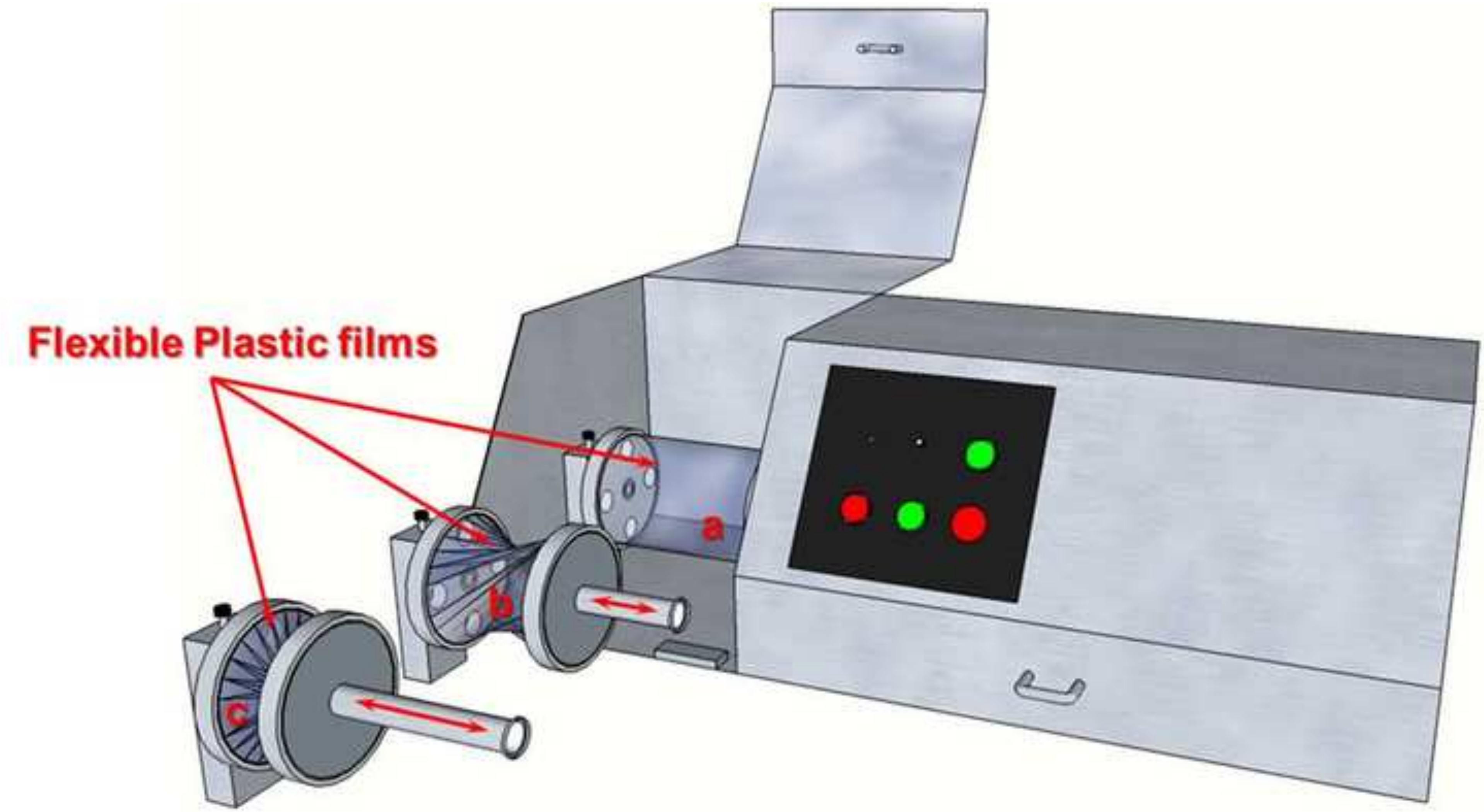

Figure2
Click here to download high resolution image

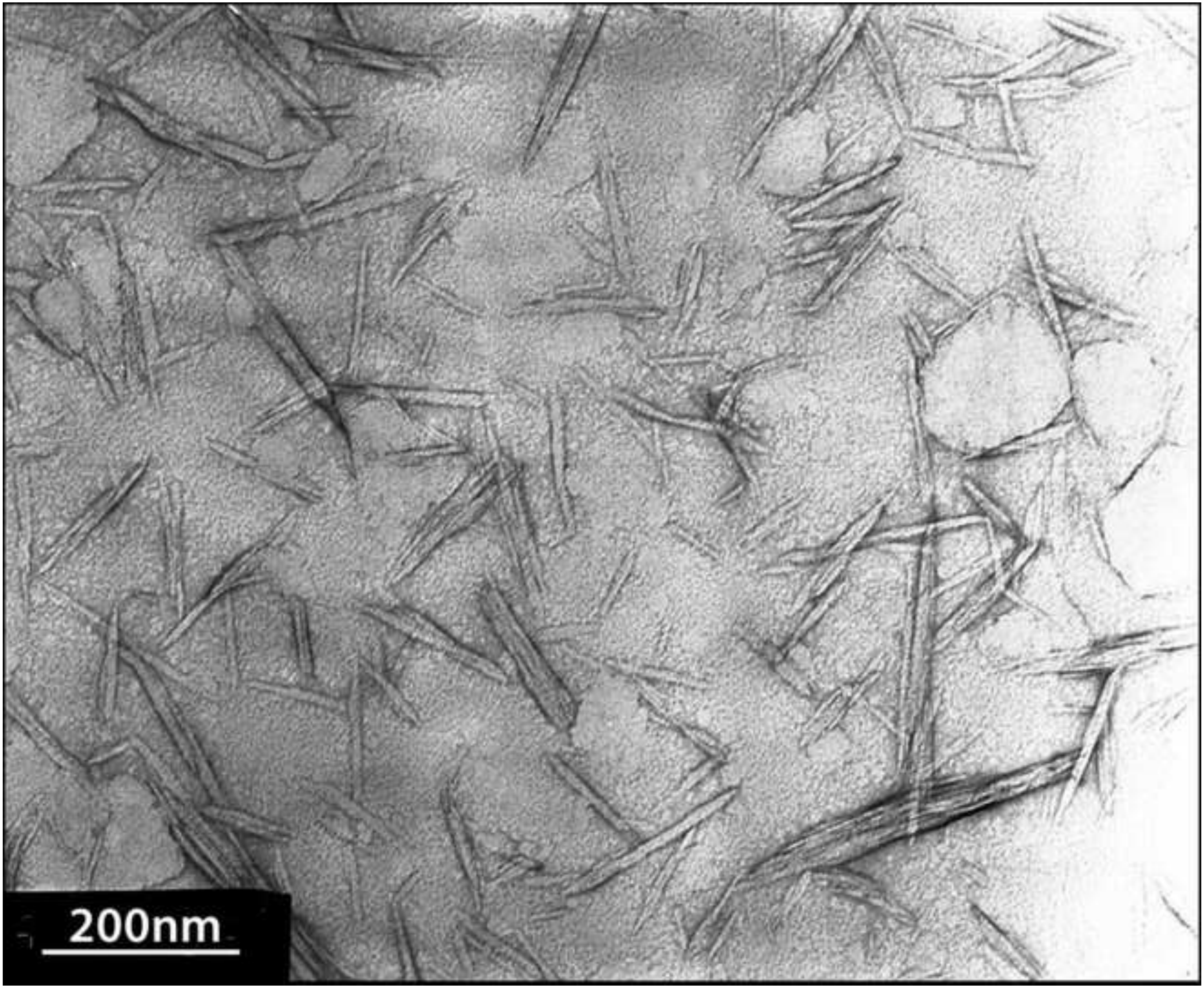

Figure3
Click here to download high resolution image

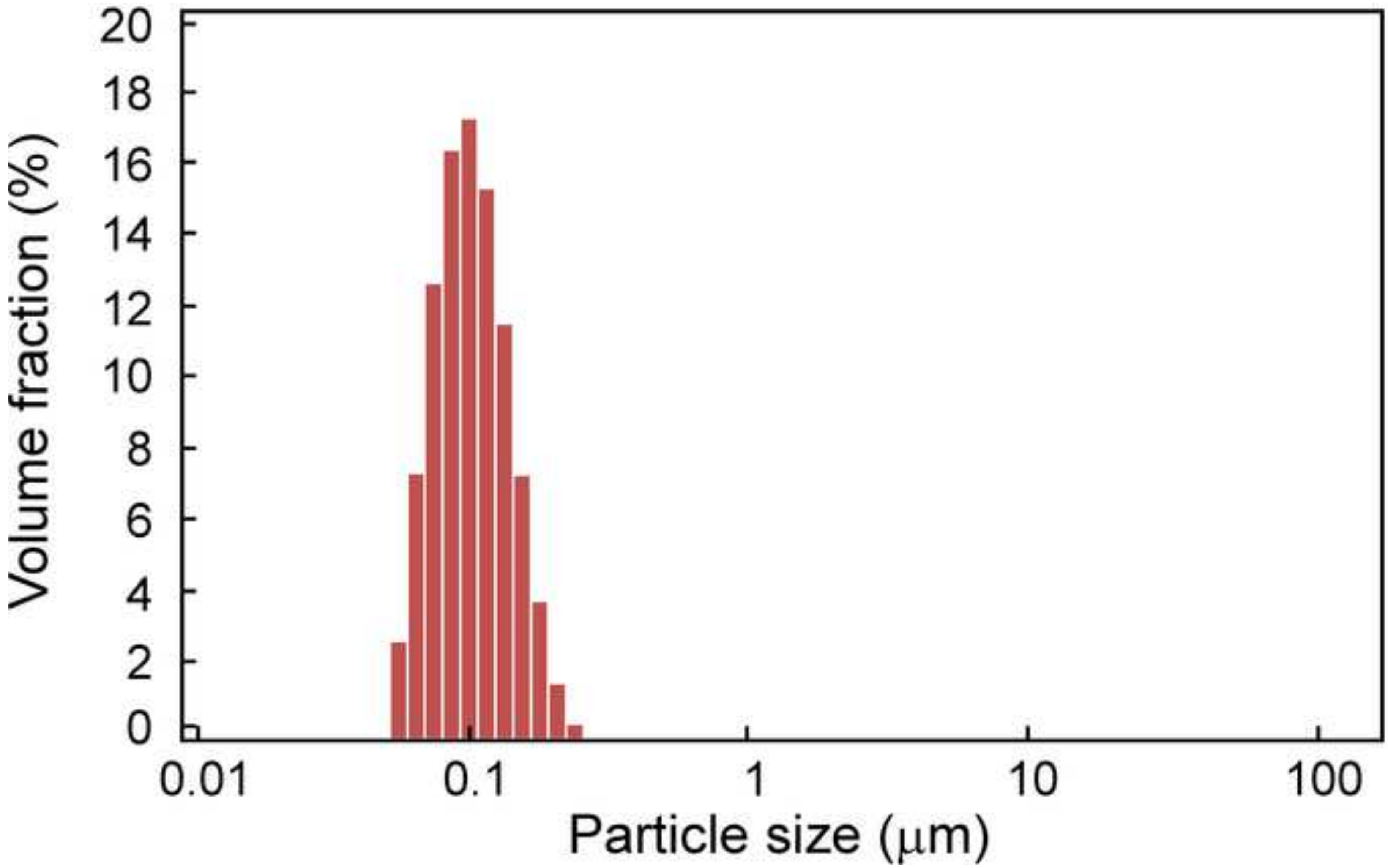

Figure4
Click here to download high resolution image

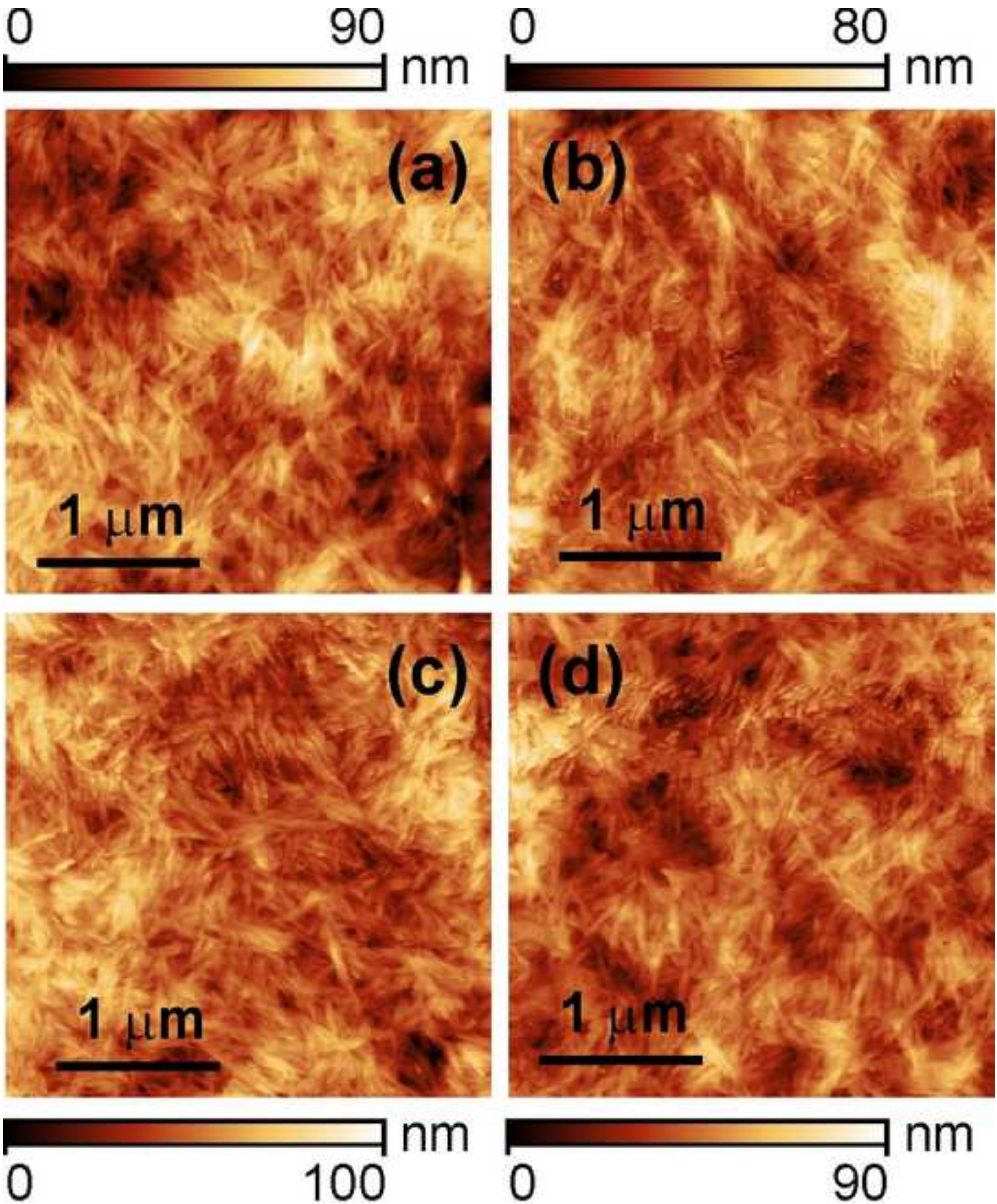

Figure5

Click here to download high resolution image

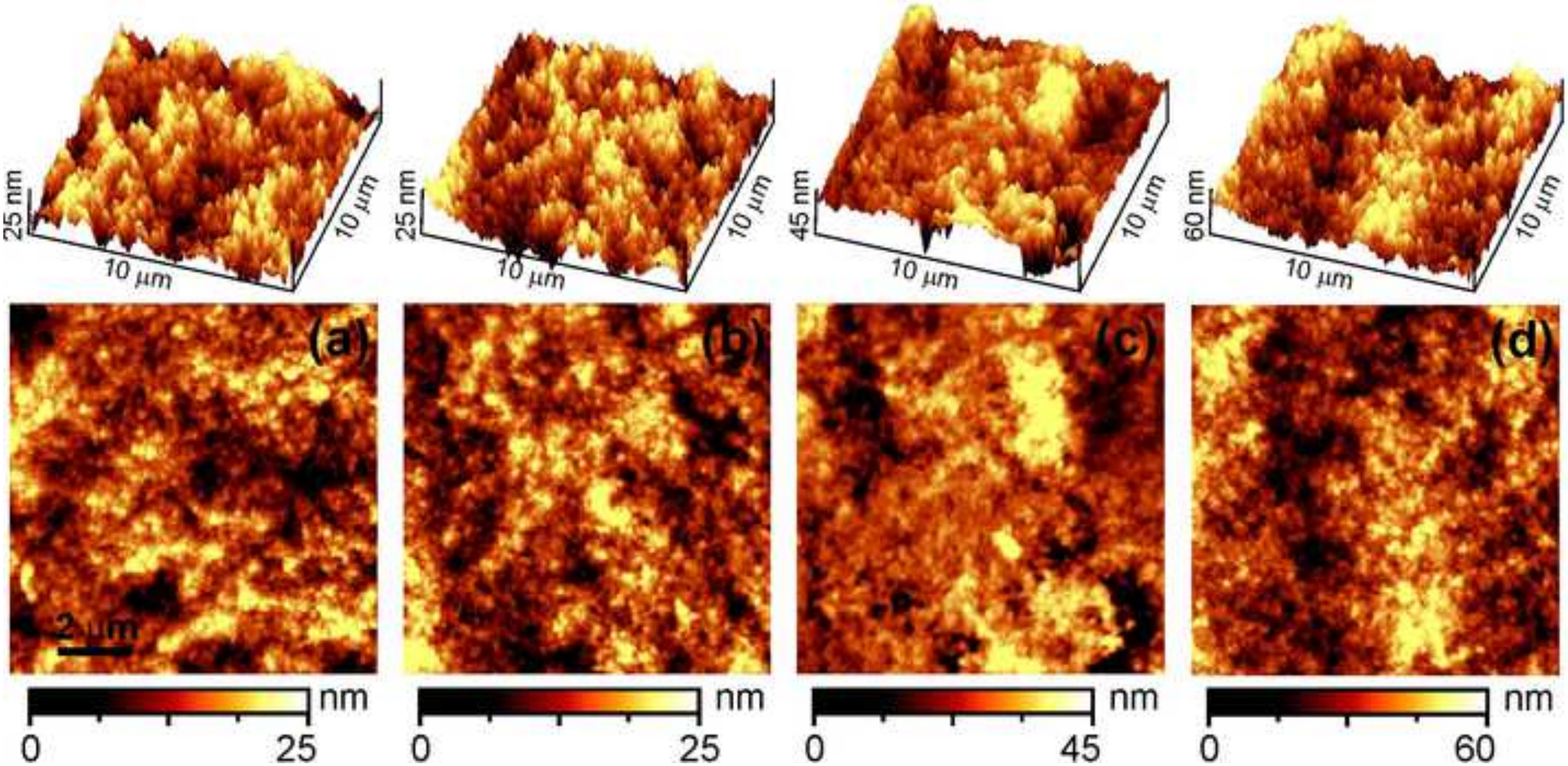

Figure6

Click here to download high resolution image

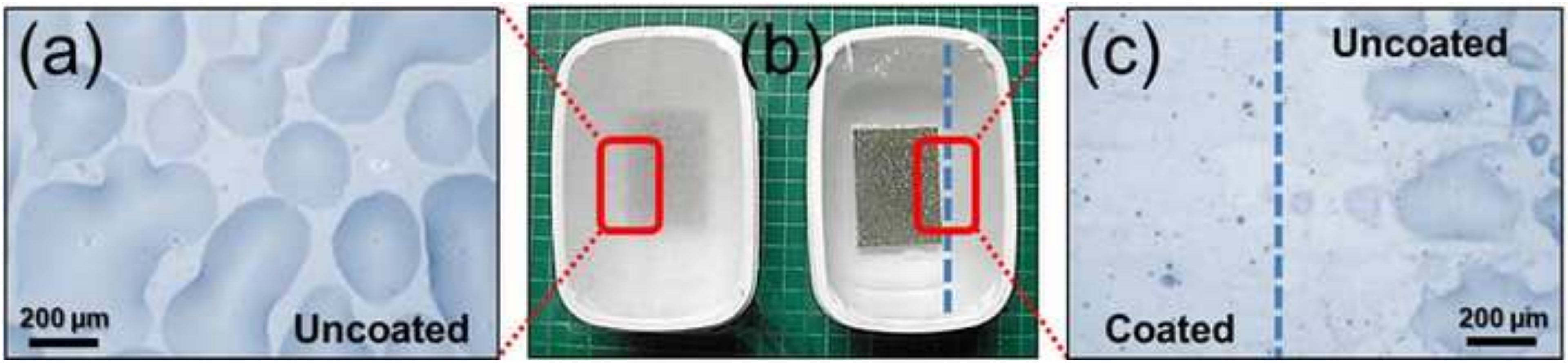

Figure7
Click here to download high resolution image

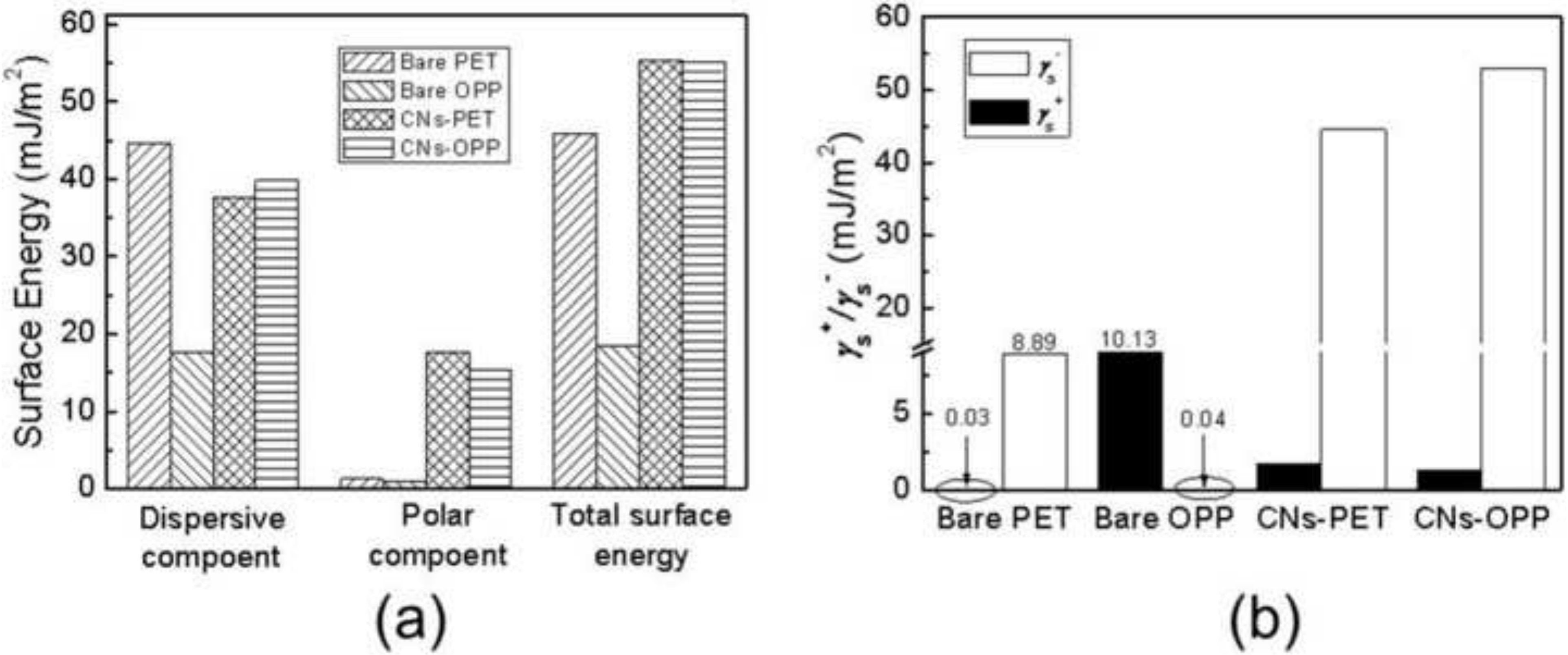

Figure8

Click here to download high resolution image

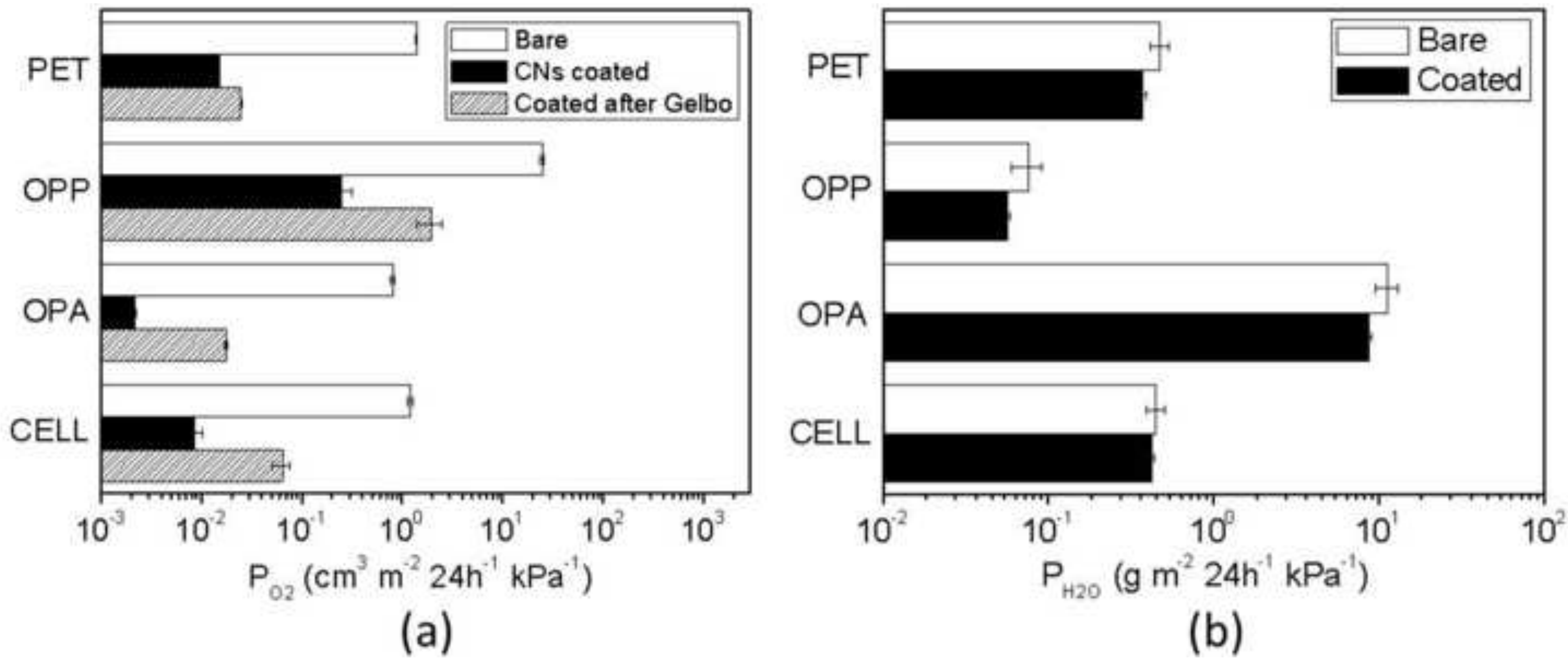

Figure9

Click here to download high resolution image

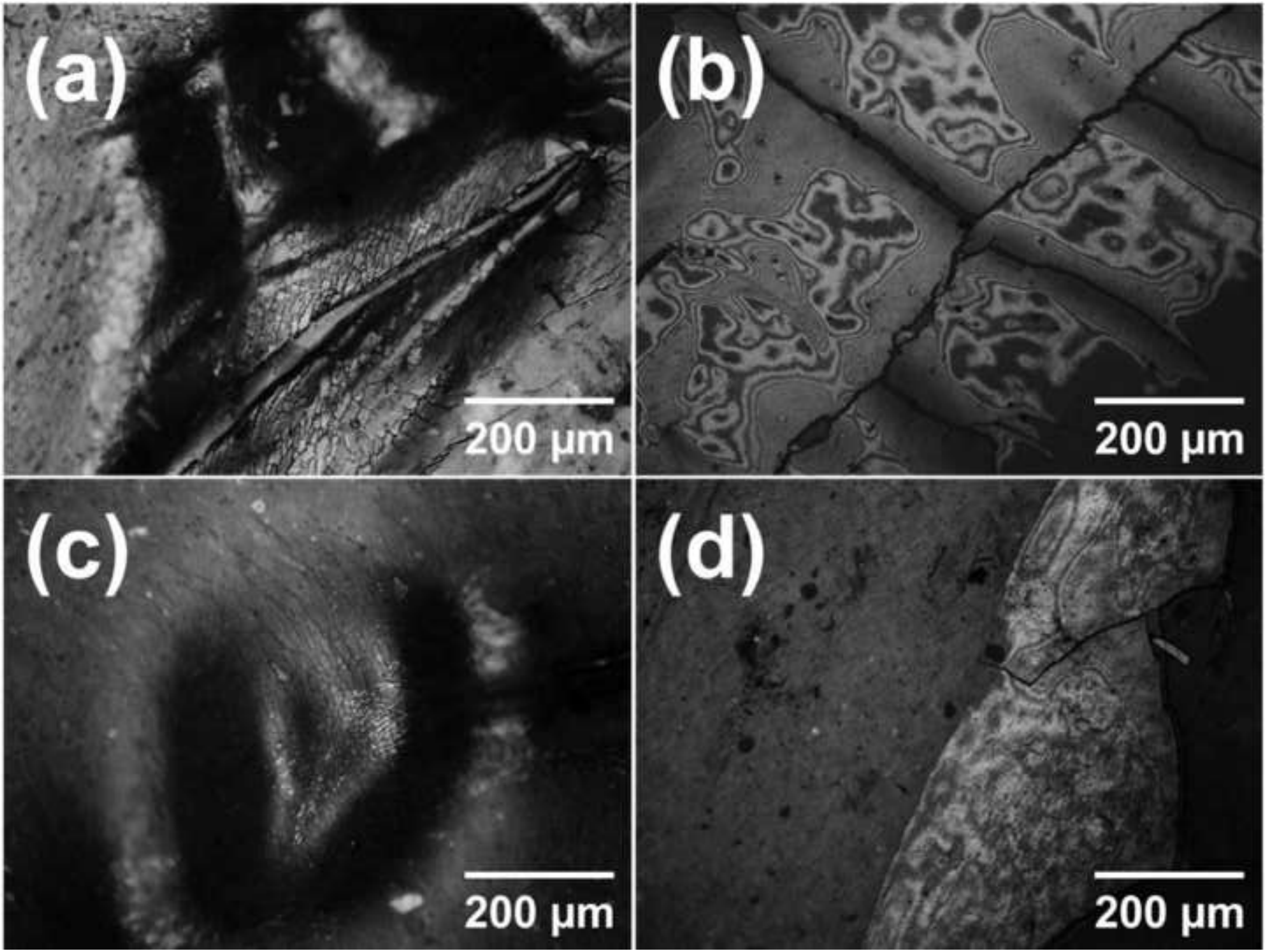

Table 1 Surface tension components and parameters of the liquids used in direct contact angle determination in mJ m^{-2}, at 20 °C (van Oss et al., 2001, van Oss, 2003)

Liquid	γ_l	γ_l^D	γ_l^P	γ_l^+	γ_l^-
APOLAR					
Diiodomethane	50.8	50.8	0	≈0.01	0
POLAR					
Water	72.8	21.8	51.0	25.5	25.5
Formamide	58.0	39.0	19.0	2.28	39.6

Table 2 The coefficient of friction (COF) of Plastic films (Ex) against plastic film (In)

Substrate	Bare (Ex)		Coated (600 nm[a])	
	μ_s	μ_d	μ_s	μ_d
PET	0.57±0.02[D]	0.52±0.03[H]	0.38±0.01[C]	0.33±0.01[G]
OPP	0.18±0.01[A]	0.17±0.00[F]	0.30±0.02[B]	0.18±0.01[F]
OPA	0.79±0.02[E]	0.74±0.03[J]	0.32±0.01[BC]	0.32±0.02[G]
CELL	0.62±0.03[D]	0.57±0.01[I]	0.38±0.02[C]	0.34±0.01[G]

[a] Thickness of CNs coating

[A] to [E], different letters mean that static COFs are significantly different (p<0.01);

[F] to [J], different letters mean that dynamic COFs are significantly different (p<0.01).

Table 3 Transparency at 550 nm and haze of bare and CNs-coated films

Substrates	Transparency (%)		Haze (%)	
	Bare	CNs-coated	Bare	CNs-coated
PET	87.5±0.3	89.0±0.3	2.9±0.1	3.3±0.2
OPP	91.8±0.0	90.8±0.2	2.1±0.0	3.4±0.3
OPA	90.2±0.5	89.8±0.0	3.0±0.1	4.0±0.2
Cellophane	87.3±0.1	88.3±0.1	3.2±0.1	3.8±0.2

Table 4a Static contact angles of bare and CNs-coated films

Films	Static CA[a]		
	θ_{Water}(°)	θ_{DIM}(°)[b]	θ_{FOM}(°)[c]
Bare PET	57.44±5.84	22.41±2.73	39.55±1.77
Bare OPP	63.03±1.00	52.22±1.61	41.39±1.70
CNs-PET	12.32±1.33	37.15±3.02	7.41±1.33
CNs-OPP	12.08±0.95	36.37±1.70	8.78±0.73

Table 4b Advancing and receding contact angles of bare and CNs-coated films

Films	Advancing CA			Receding CA		
	θ_{Water}(°)	θ_{DIM}(°)[b]	θ_{FOM}(°)[c]	θ_{Water}(°)	θ_{DIM}(°)[b]	θ_{FOM}(°)[c]
Bare PET	72.57±2.96	29.00±2.12	50.27±2.97	25.34±2.12	8.16±0.82	14.30±2.76
Bare OPP	90.06±1.84	79.72±0.69	52.99±2.65	17.18±3.41	22.72±1.26	11.23±1.38
CNs-PET	26.29±3.27	43.91±2.03	17.10±0.74	8.56±2.23	8.20±0.34	6.79±2.01
CNs-OPP	27.33±3.07	39.56±2.50	17.30±2.94	5.63±0.45	7.21±4.63	5.58±2.33

[a] static contact angle values recorded at 60th second

[b] DIM, diiodomethane

[c] FOM, formamide,